

1 **Local skin inflammation in cutaneous leishmaniasis as a source of variable**
2 **pharmacokinetics and therapeutic efficacy of liposomal amphotericin B**

3 Gert-Jan Wijnant^{1,4}, Katrien Van Bocxlaer¹, Amanda Fortes Francisco², Vanessa Yardley¹, Andy
4 Harris³, Mo Alavijeh³, Sudaxshina Murdan⁴ and Simon L. Croft¹

5

6 1. Department of Immunology and Infection, Faculty of Infectious and Tropical Diseases, London School of
7 Hygiene and Tropical Medicine, London, United Kingdom

8 2. Department of Pathogen Molecular Biology, Faculty of Infectious and Tropical Diseases, London School
9 of Hygiene and Tropical Medicine, London, United Kingdom

10 3. Pharmidex Pharmaceutical Services Ltd, 3rd floor, 14 Hanover Street, London, United Kingdom

11 4. Department of Pharmaceutics, UCL School of Pharmacy, London, United Kingdom

12

13 Corresponding author simon.croft@lshtm.ac.uk

14

15

16

17

18

19

20

21

22

23

24

25

26 **ABSTRACT**

27 Disfiguring skin lesions caused by several species of the *Leishmania* parasite characterize cutaneous
28 leishmaniasis (CL). Successful treatment of CL with intravenous (IV) liposomal amphotericin B
29 (LAmB) relies on the presence of adequate antibiotic concentrations at the dermal site of infection
30 within the inflamed skin. Here, we have investigated the impact of the local skin inflammation on the
31 pharmacokinetics (PK) and efficacy of LAmB in two murine models of localized CL (*Leishmania major*
32 and *Leishmania mexicana*) at three different stages of disease (papule, initial nodule and established
33 nodule). Twenty-four hours after administration of 1 x 25 mg/kg LAmB (IV) to infected BALB/c mice
34 (n=5), drug accumulation in skin was found to be dependent on the causative parasite species (*L.*
35 *major* > *L. mexicana*) and the disease stage (papule > initial nodule > established nodule > healthy
36 skin). Elevated tissue drug levels were associated with increased vascular permeability (Evans Blue
37 assay) and macrophage infiltration (histomorphometry) in the infected skin, two pathophysiological
38 parameters linked to tissue inflammation. After identical treatment of CL in the two models with 5 x 25
39 mg/kg LAmB (IV), intralesional drug concentrations and reductions in lesion size and parasite load
40 (qPCR) were all \geq 2-fold higher for *L. major* compared to *L. mexicana*. In conclusion, drug penetration
41 of LAmB into CL skin lesions could depend on the disease stage and the causative *Leishmania*
42 species due to the influence of local tissue inflammation.

43

44 **KEYWORDS**

45 Cutaneous leishmaniasis, inflammation, pharmacokinetics, liposomal amphotericin B

46

47 **INTRODUCTION**

48 Leishmaniasis is a vector-borne neglected tropical disease caused by over 20 distinct species of the
49 protozoan *Leishmania* parasite. The two main forms, visceral (VL) and cutaneous leishmaniasis (CL),
50 continue to pose a major public health problem with significant socioeconomic burden worldwide (1).
51 Current estimates show a global annual incidence of one million, 12 million prevalent cases in 98
52 countries and over 350 million people at risk of infection (2). CL presents as a wide clinical spectrum
53 of skin syndromes, ranging from severe and rare mucosal (MCL), diffuse (DCL) or chronic to the more

54 common, uncomplicated localized (LCL) lesions. In LCL, single or a limited number of lesions form at
55 the bite site of the parasite-infected female sand fly. A small papule forms, which develops into an
56 initial nodule and then an established nodule with signs of exudation and/or crust formation. The
57 nodule progressively ulcerates and eventually leaves an open wound with raised borders and a
58 crater-like appearance. In most cases, such ulcers slowly self-heal, but leave permanent, disfiguring
59 scars on the exposed skin areas that are often the cause of serious social stigma (3). Tissue damage
60 and disease in CL are primarily caused by an excessive host immune response against the
61 intracellular infection of dermal macrophages by *Leishmania* (4). As the dermis fills with a dense and
62 diffuse mixed inflammatory cell infiltrate (including macrophages, lymphocytes, neutrophils, mast cells
63 and plasma cells), the associated oedema drives swelling of the tissue. Epidermal changes
64 (hyperkeratosis, acanthosis and degeneration of the basal layer), connective tissue damage (collagen
65 lysis) and the formation of non-caseating granuloma can occur (5-9). The immunopathology of LCL
66 shows both similarities (chronic, often ulcerative, dermatosis) and differences (clinical presentation,
67 incubation and resolution time) among different causative *Leishmania* species (10, 11). For example,
68 Old World *L. major* causes so-called 'wet' and acute (early ulcerative) CL lesions in the Middle East:
69 large, irregular and often oozing wounds, which rapidly progress and heal over two to six months (12,
70 13). In Central America, New World *L. mexicana* is the responsible agent for "chiclero's ulcers",
71 chronic lesions typically found on the ear which spontaneously re-epithelize over a period lasting
72 months to even years (14, 15). In a minority of CL cases caused by *L. major* and *L. mexicana*,
73 alternative types of skin lesions with different clinical presentations and immune response can
74 develop (12-15).

75 Treatment of CL is problematic; long series of painful injections with the toxic pentavalent antimonials
76 remain the standard therapy (16). A better tolerated, but expensive second-line drug requiring
77 intravenous (IV) administration and cold chain, is AmBisome® (LAmB) (17). LAmB is a unilamellar
78 liposomal formulation of the polyene antibiotic amphotericin B (AmB), which forms cidal pores in the
79 leishmanial cell membranes by ergosterol binding (18). Several treatment regimens for a total
80 cumulative dose of 20-25 mg/kg are efficacious against CL and MCL (19). However, therapeutic
81 responses vary for the different causative *Leishmania* species, populations, geographical regions and
82 clinical settings (20).

83 We have recently demonstrated that the efficacy of LAmB in murine CL relies on adequate exposure
84 of the active compound amphotericin B (AmB) at the local site of infection, the skin lesion. Moreover,
85 we also showed higher drug disposition in diseased compared to healthy skin (21). Altered
86 pharmacokinetics (PK) at sites of tissue inflammation have been reported previously for antimicrobials
87 (22), anti-inflammatory agents (23) and cancer chemotherapeutics (24). Based on these observations,
88 we formulated three hypotheses.

89 First, the preferential drug distribution of LAmB in CL lesions over uninfected skin can be explained by
90 the presence and the severity of the local skin inflammation. This could vary among different disease
91 stages of CL and among causative parasite species. In the context of LCL skin inflammation, we have
92 focussed only on aspects potentially relevant to the pharmacological action of liposomal drugs. The
93 inflammatory response against the *Leishmania* infection at the skin inoculation site involves increased
94 vascular permeability and vasodilatation of dermal blood vessels and the infiltration of several types of
95 immune cells including macrophages that play a role in tissue swelling and the formation of skin
96 lesions. Second, the underlying mechanisms for altered drug distribution at the inflammatory site are,
97 at least in part, local capillary leakiness (25-28) and influx of drug-loaded macrophages into the skin
98 (29-34). Third and final, AmB levels accumulating in lesions following LAmB treatment can be source
99 of variability in treatment outcomes against different *Leishmania* species. To test the first two
100 hypotheses, we studied the skin PK of LAmB after administration of a single high dose (1 x 25 mg/kg,
101 IV), as well as pathophysiological parameters that could influence the drug distribution process from
102 blood to skin using the Evans Blue assay (35-37) and histomorphometry. This was done in infected
103 mice and in control mice with variable degrees of skin inflammation: none (uninfected), high
104 (pseudolesion PL, a new mouse model of local skin inflammation based on the rat paw oedema
105 model (38, 39)), or low (healed lesion HL, cure of CL by paromomycin sulphate (40)). Figure 1 gives
106 an overview of the experimental groups and procedures. To investigate the third hypothesis, we
107 compared intralesional drug accumulation and efficacy in *L. major* and *L. mexicana* murine CL
108 following treatment with an identical LAmB dose regimen (5 x 25 mg/kg, IV).

109

110 RESULTS

111 **Pharmacokinetic arm: AmB accumulation in skin after LAmB administration.**

112 Figure 2 shows AmB accumulation (ng AmB per gram skin tissue; ng AmB per lesion) in infected and
113 healthy control skin at different stages of murine *L. major* or *L. mexicana* CL (papule, initial nodule,
114 established nodule) 24 hours after administration of a single dose of 25 mg/kg LAmB (IV). The
115 morphology of the lesions is shown in figure 6 (panel a). Table 1 shows AmB lesion-to-healthy-skin-
116 ratios, the ratio of the AmB skin level in the lesion over the AmB skin levels in the healthy control skin
117 (calculated from values in figure 2, row 1). The ratios indicate that there is a 3-fold decrease of
118 intralésional AmB accumulation when LAmB is administered at late (established nodule) compared to
119 early (papule) stages of both *L. major* and *L. mexicana* CL. Drug levels were higher in *L. major* than in
120 *L. mexicana* lesions at all stages of disease. Disposition of AmB in the PL was significantly higher
121 than in healthy skin ($p < 0.0001$). In contrast, AmB accumulation in HL is not significantly different to
122 that in healthy control skin ($p = 0.37$) and is similar to the baseline levels in uninfected mice. Drug
123 distribution patterns are highly comparable when AmB concentrations are expressed relative
124 (normalized, ng/g) or absolute (ng/lesion). This indicates that the altered PK of LAmB at different
125 stages of CL is not a consequence of bias introduced by change in tissue volume/weight over the
126 course of infection.

127 **Skin pathophysiology arm: factors affecting the PK of LAmB.**

128 **Lesion characterisation: size and parasite load.** Figure 3 shows the lesion characteristics (top row:
129 lesion size, bottom row: parasite load) at different stages of infection by *L. major* or *L. mexicana* CL
130 (papule, initial nodule, established nodule). The morphology of the lesions can be seen in figure 6
131 (panel a). *L. major* lesions increased in size at a more rapid pace than *L. mexicana*, with different
132 parasite load dynamics over time. During the 20 days following infection with *L. major*, lesion size
133 gradually increased from 0 to around 7 mm and parasite load remained stable from day 5. Following
134 infection with *L. mexicana*, smaller lesions formed (up to 5 mm) and the parasite load gradually
135 increased. The PL swelling of rump skin had a size comparable to CL lesions, but as expected, no
136 parasites could be detected in this *Leishmania*-free type of skin inflammation. In contrast, the HL (day
137 20, after 10-day treatment with paromomycin) had a lesion size of 0 ± 0 mm and parasite load was
138 around a 100-fold lower than in the untreated *L. major* established nodules (day 20). As expected,
139 neither lesion size nor parasite load was measurable in uninfected mice.

140 **Evans Blue: leakiness of dermal capillaries.** Figure 4 shows vascular permeability in infected and
141 healthy control skin at different stages of murine *L. major* or *L. mexicana* CL (papule, initial nodule,
142 established nodule), as evaluated by the Evans Blue Assay. The morphology of the lesions can be
143 seen in figure 6 (panel a). Table 1 shows Evans Blue lesion-to-healthy-skin-ratios, the ratio of the
144 Evans Blue skin level in the lesion over the Evans Blue skin levels in the healthy control skin
145 (calculated from the values in figure 4). The ratios for *L. major* indicate that, compared to healthy
146 control skin, vascular permeability is 6-fold higher in papules and 9-fold higher in initial nodules and
147 established nodules. For *L. mexicana*, there is 3-10 fold increase in permeability compared to healthy
148 skin and the increase is comparable at papular, nodular and established nodulative stages. Blood
149 vessel leakiness was 12-fold higher ($p < 0.0001$) in the PL than in healthy skin. In HL, vascular
150 permeability is not significantly different to that in healthy control skin ($p = 0.99$) and is similar to the
151 baseline levels in uninfected mice. In the photos in figure 4, the intense blue coloration of lesions (due
152 to accumulation of the dye Evans Blue) provides an additional, qualitative confirmation of capillary
153 leakiness at the site of infection. Such a phenomenon is absent in healthy skin tissues.

154 **Skin histomorphometry: inflammatory cells and macrophages.** Figure 5 shows the number of
155 total cells (top row) and the abundance of macrophages (bottom row) in infected and healthy control
156 skin at different stages of murine *L. major* or *L. mexicana* CL (papule, initial nodule, established
157 nodule). Figure 6 shows the morphology of the lesions (panel a), the H&E stain (panel b) and the anti-
158 Iba-1 stain (panel c). Figure 7 examines the H&E and Iba-1 stains of CL lesions in more detail. Table
159 1 shows total cell and macrophage lesion-to-healthy-skin-ratios, the ratio of the total cell and
160 macrophage skin numbers in the lesion over the total cell and macrophage skin numbers in the
161 healthy control skin (calculated from the values in figure 5). The ratios indicate that the number of
162 cells in the tissue doubles in CL lesions as the disease progresses and a large fraction of the
163 infiltrated inflammatory cells are macrophages. However, the number of inflammatory cells and
164 macrophages in *L. major* lesions are higher than those in *L. mexicana* lesions at all stages of disease.
165 In the PL, the number of inflammatory cells were significantly higher than in healthy skin ($p = 0.0034$),
166 but this was not the case for macrophages specifically ($p > 0.99$). In the HL, the number of
167 inflammatory cells and macrophages were not significantly different to that in healthy control skin
168 ($p > 0.05$) and are similar to the baseline levels in uninfected mice.

169 **Relation between PK and pathophysiology parameters.** Table 1 shows the lesion-over-healthy-
170 skin-ratios (parameter value in lesion / parameter value in healthy skin) for AmB accumulation (figure
171 2 data, AmB levels in ng/g), blood vessel permeability (figure 4 data), number of cells and number of
172 macrophages (figure 5 data). For uninfected mice, the ratios for AmB, blood vessel permeability, cell
173 numbers and macrophage numbers were around 1, indicating no difference in the values for these
174 parameters between the lesion site (rump skin) and the healthy site (back skin). Comparing
175 *Leishmania*-infected mice to uninfected mice, AmB accumulation, blood vessel permeability, cell
176 numbers and macrophage numbers were higher at all three stages of disease for both *L. major* and *L.*
177 *mexicana*. However, these ratios were increased for *L. major* compared to *L. mexicana*. The higher
178 ratios for PL compared to uninfected mice indicate increased drug accumulation as well as blood
179 vessel leakiness, cell numbers and macrophages in this alternative type of skin inflammation. For HL,
180 however, all lesion-over-healthy ratios were highly similar to the baseline ratios found in healthy mice
181 (except for macrophage number). Similar patterns at different stages of disease were found in *L.*
182 *major* and *L. mexicana*-infected mice. A significant increase in ratios for drug accumulation, blood
183 vessel permeability, cell numbers and macrophage numbers was found in papules (early CL)
184 compared to uninfected mice. Comparing ratios for the papule compared to those for initial nodules
185 and established nodules (later-stage CL), relatively little new, additional inflammatory cells and
186 macrophages seemed to infiltrate the skin (for both *L. major* and *L. mexicana*) and blood vessel
187 permeability remained stable (for *L. major* but not *L. mexicana*).

188 **Skin PK and efficacy of LAmB in CL.**

189 Finally, we evaluated the efficacy of LAmB against *L. major* and *L. mexicana* in the BALB/c mouse
190 model of CL. Figure 8 shows *in vivo* activity and intralesional AmB accumulation on day 10, after
191 treatment of mice with initial nodules with 5 doses of 25 mg/kg LAmB (IV) on alternate days (i.e. on
192 day 0, 2, 4, 6 and 8). LAmB showed *in vivo* activity against both CL-causing parasite species.
193 However, reductions in lesion size and parasite load compared to untreated controls were greater and
194 significant for *L. major* ($p=0.011$ and 0.0471) compared to *L. mexicana* ($p=0.25$ and 0.99). We also
195 observed almost 2-fold higher AmB levels (ng/g) in *L. major* over *L. mexicana* lesions. In CL-infected
196 skin, drug levels concentrations were at least 4-fold higher comparing to healthy rump skin of
197 identically uninfected LAmB treated mice. However, this difference was significant for *L. major*

198 ($p < 0.0001$) but not for *L. mexicana* ($p = 0.15$). The *L. major* data has already been reported earlier (21),
199 but is included to enable direct comparison with *L. mexicana* (novel data).

200

201 DISCUSSION

202 Local tissue inflammation in infectious disease can alter the pharmacokinetics (PK) and thus
203 therapeutic outcomes of antimicrobials (41-43). In this work, we have confirmed our hypothesis that
204 the inflamed state of skin lesions in CL alters the PK of liposomal amphotericin B (LAmB) following
205 intravenous drug administration in two mouse models of infection. Our results show that AmB
206 accumulation in CL-infected skin is (i) *Leishmania* species-specific (*L. major* > *L. mexicana* lesions)
207 (ii) disease-stage-specific (papule > initial nodule > established nodule > healthy skin) and (iii) a
208 plausible cause of the superior *in vivo* efficacy of LAmB against *L. major* compared to *L. mexicana*.

209 Firstly, the preferential distribution of LAmB to CL infection sites (*L. major* > *L. mexicana*) compared to
210 uninfected ones could be explained by the presence and the severity of the local inflammatory
211 response against the parasites residing in dermal macrophages. Compared to *L. mexicana*, *L. major*
212 causes more heavily inflamed (exudative) established nodules with a more rapid, aggressive onset in
213 humans (12-15) and mice (3, 44). Several quantitative biomarkers for skin inflammation in our study
214 confirmed this. Leakiness of the dermal capillaries, swelling/oedema in the skin tissue (indicated by
215 lesion size) and numbers of infiltrating macrophages or other inflammatory cells were higher in *L.*
216 *major* compared to *L. mexicana* CL, at all stages of disease. These findings are consistent with earlier
217 reports (45-47). Moreover, the HL and PL observations support this inflammation-driven theory of
218 enhanced drug accumulation. When the inflammation in *L. major*-infected skin is largely cleared
219 because of parasite elimination by paromomycin treatment (HL), AmB accumulation, blood vessel
220 permeability and cell numbers return to baseline levels seen in uninfected skin. However, when
221 inflammation is experimentally induced by injection of λ -carrageenan (instead of parasites) in rump
222 skin (similar site as in CL-infection), the local drug concentrations after LAmB administration also
223 increase by over 3-fold. Such a phenomenon could be explained by a 10-fold increase in leakiness of
224 the skin capillaries. The new PL model of local skin inflammation, based on subcutaneous injection of
225 λ -carrageenan, could be a useful research tool for dermatoses other than CL, such as skin cancers,
226 atopic dermatitis or psoriasis (48).

227 Secondly, the increased intralesional AmB accumulation after intravenous LAmB dosing of mice with
228 CL in earlier stages of disease (papule > initial nodule > established nodule) could be related to
229 changes in infiltration of phagocytes prone to internalize circulating liposomes and, likely to lesser
230 degree, capillary leakiness in the dermis. When LAmB is administered to mice with early CL, during
231 the initial massive influx of phagocytes and inflammatory cells into the skin as part of the
232 antileishmanial immune response (4, 11), intralesional drug levels could be increased as AmB-loaded
233 cells migrate from the blood stream to the infection site. Hence, in later stages of disease, when the
234 number of additional macrophages infiltrating the infected tissue is more limited, skin AmB
235 accumulation could be lower. The known role of phagocyte transport in the delivery of various
236 antibiotics (30-32), including liposomal AmB (41), to local infection sites, as well as our PK and
237 histology data suggests the plausibility of this hypothesis. Confirmative research should distinguish
238 extra- and intracellular levels in circulating and dermal macrophages after LAmB administration. While
239 phagocytes can increase AmB exposure in the lesion, their therapeutic relevance is still unclear.
240 Cellular lysis, resulting in local release of the drug payload, or impaired parasite survival in these
241 'pretreated' macrophages could play a role. Another pathophysiological factor affecting the PK of
242 LAmB is blood vessel leakiness, a result of vasodilatation and enhanced vascular permeability in the
243 inflamed dermis. Here, we confirmed the existence of this phenomenon in experimental CL for the
244 first time. It could facilitate extravasation of the liposomes (~ 80 nm in size) through the dermal
245 capillaries, which under normal physiological conditions have a pore cut-off size of 6-12 nm (21).
246 However, it cannot explain a decrease in AmB disposition in lesions as CL progresses by itself,
247 because we found comparable degrees of capillary leakage similar in papules, initial nodules and
248 established nodules. Other factors that could affect cellular and dermal PK, such as plasma and
249 tissue protein-binding (49), angiogenesis (50), lymphatic drainage, phagocytic capacity and activation
250 stage of (parasitized) macrophages (33), skin metabolism, clearance by the reticuloendothelial
251 system (51), or the involvement of (non-macrophage) immune cells, mediators or responses, were not
252 evaluated in this study. A similar trend of decreasing drug distribution of LAmB to target organs during
253 later disease stages was also found in murine VL (33). However, interestingly, *Leishmania*-infected
254 livers contain lower rather than higher drug levels compared to healthy ones.

255 Thirdly, the *in vivo* activity of LAmB was superior against *L. major* compared to *L. mexicana*, likely due
256 to inflammation-enhanced and relatively increased drug levels at the infection site. A clear correlation

257 between drug levels of the leishmanicidal, concentration-dependent antibiotic AmB delivered to the
258 lesion and the efficacy of LAmB in murine CL has already been reported (21, 52). Apart from skin PK,
259 there could be also be differences in antileishmanial pharmacodynamics (PD) and the resulting
260 PK/PD relationship. An intrinsic species-specific sensitivity to the active compound AmB is unlikely, as
261 *in vitro* EC₅₀ values are comparable ($\approx 0.1 \mu\text{M}$) (35). However, the *in vivo* susceptibility could still vary
262 based on the metabolic state of the *L. major* or *L. mexicana* parasites in the skin. In chronic lesions
263 with slow disease onset, a quiescent, semi-dormant phenotype of *L. mexicana* could exist, benefitting
264 its long-term survival and possibly showing reduced drug sensitivity (53-55). Such PK/PD factors
265 could cause variable rate or magnitude of parasite elimination, a combined outcome of drug activity
266 and host immunity. Pharmacogenetic differences between individual patients and populations
267 (affecting distribution, metabolism and clearance) might also contribute to additional variation in LAmB
268 efficacy in the clinic (20).

269 Finally, although BALB/c mice are common in PK studies (56) and *L. major*-BALB/c is a highly
270 reproducible and well-established model for antileishmanial drug evaluation (57), differences between
271 CL in humans (mostly self-curing lesions) and BALB/c mice (non-healing lesions) (58) should be
272 considered. Our studies used mice with relatively small ($< 1 \text{ cm}$), local and uncomplicated CL lesions.
273 Despite variation in the immunological nature of the skin inflammation, the phenomena of capillary
274 leakiness, oedema formation and phagocyte infiltration occur in both mice and humans (59, 60).
275 Thus, our findings could hold treatment implications for CL as well as for other inflammatory (skin)
276 disorders. During preclinical evaluation of novel nanoparticles, a drug delivery strategy used for CL
277 (61), the time of drug administration (relative to disease stage) and causative species are important
278 factors that can affect both PK and PD. In the clinic, LAmB treatment outcomes in CL are already
279 known to relate to the causative *Leishmania* species. A recent observational study in a group of
280 travellers with (M)CL (20) reported differences in the therapeutic success rate of LAmB against *L.*
281 *infantum* (78%), *L. major* (50%) and *Leishmania Viannia* subgenus species (28%). However, because
282 *L. mexicana* was not included in this work, we can not directly compare our results in mice to those in
283 humans. In addition, early diagnosis and therapeutic intervention with LAmB could produce enhanced
284 drug exposure in the skin lesion. No present clinical studies have reported on this. In contrast, early
285 treatment of *L. brasiliensis* CL with intramuscular pentavalent antimonials was associated with a 5-
286 fold increased risk of treatment failure (62, 63). Both the impact of parasite species and the age of the

287 lesion in CL on PK and therapeutic efficacy of LAmB (and other antileishmanial drugs) deserve further
288 investigation. Laboratory experiments could investigate outcomes of multi-dose treatments in
289 alternative models of disease caused by additional *Leishmania* species and strains. Extrapolation of
290 LCL results to the various types of complex CL is complicated by differences in histopathology (blood
291 vessel destruction in advanced MCL (10)) and the nature and severity of the inflammatory response
292 (balance TH1/TH2-type cellular immunity in local *versus* diffuse CL (3, 4)). Overall, it is clear that the
293 immunohistopathology of CL has a profound impact on drug disposition of antileishmanial agents,
294 both when administered topically (increased permeation through the damaged epidermis (64, 65))
295 and systemically (enhanced extravasation for liposomal and non-encapsulated drugs (21)).

296 In conclusion, our data indicates that the severity of inflammatory skin disease in CL could contribute
297 to variable drug penetration in the target tissue and therapeutic efficacy of LAmB. The significant
298 impact of local inflammation on PK and PK/PD is not only an important consideration for the
299 development of new drugs and clinical dose regimens for the treatment of CL, but also for other
300 (infectious) diseases with an inflammatory component.

301

302 MATERIALS AND METHODS

303 **Parasites, media and drugs.** *L. major* MHOM/SA85/JISH118 and *L. mexicana* MNYC/BZ/62/M379
304 parasites were cultured in Schneider's insect medium (Sigma, UK) supplemented with 10% heat-
305 inactivated fetal calf serum (HiFCS, Sigma UK). These were passaged each week at a 1:10 ratio of
306 existing culture to fresh media in 25 ml culture flasks without filter and incubated at 26 °C. For
307 infection of mice, stationary phase parasites were centrifuged for 10 minutes at 2100 rpm and 4 °C.
308 The supernatant was removed and the pellet re-suspended in RPMI medium (Sigma, UK). Cell
309 number was estimated by microscopic counting with a Neubauer haemocytometer. AmBisome®
310 (LAmB, Gilead, UK) was reconstituted with 12 ml sterile water (as per the manufacturer's instructions)
311 to yield a stock solution of 4 mg/ml and diluted in 5% aqueous dextrose to achieve a drug dose of 25
312 mg/kg. Paromomycin sulphate (Sigma, UK) was prepared in phosphate buffered saline (PBS) to yield
313 50 mg/kg doses. λ-carrageenan (Sigma, UK) and Evans Blue (Sigma UK) 0.5 % (w/v) solutions were
314 made up in phosphate buffered saline (PBS, Sigma, UK). Drug preparations were stored at 4 °C
315 during the experiments.

316 **Experimental groups.** Female BALB/c mice around 6-8 weeks old and a mean weight of 18-20 g
317 were purchased from Charles River Ltd (Margate, UK). These were kept in humidity and temperature
318 controlled rooms (55-65%, 25-26 °C) and fed water and rodent food *ad libitum*. Mice were randomized
319 and allowed an acclimatization time of one week. All animal experiments were conducted under
320 license 70/8427 according to UK Home Office regulations under the Animals (Scientific Procedures)
321 Act 1986 and EC Directive 2010/63/E. An overview of the groups is shown in figure 1.

322 1. *L. major* CL. Mice were subcutaneously (SC) infected in the shaven rump above the tail with
323 200 µl parasite suspension containing 4×10^7 of low passage number ($P < 5$), stationary phase
324 *L. major* promastigotes in RPMI medium. Lesion size was measured daily with digital
325 callipers (average of length and width) after inoculation as the CL lesions developed into
326 papules, initial nodules and established nodules. In this animal model of CL, these respective
327 disease stages occurred on day 5, 10 and 20, as shown previously (40). We define a 'CL
328 lesion' as a stationary, local skin abnormality at the site of *Leishmania* parasite inoculation
329 (rump). A 'papule' is the smallest (2-4 mm) CL lesion, a palpable elevation of the skin with no
330 signs of ulceration. An 'initial nodule' is a medium-sized (4-6 mm) papule that is larger and
331 more defined. An 'established nodule' is a larger (5-8 mm) CL lesion that is crusted or
332 exudative.

333 2. *L. mexicana* CL. Mice were infected as described above for *L. major*, but *L. mexicana*
334 promastigotes were used. In this animal model of CL, the disease stages of papule, initial
335 nodule and established nodule occurred on days 15, 30 and 45 post-inoculation (40). The
336 earlier definitions of 'CL lesion', 'papule', 'initial nodule' and 'established nodule' apply.

337 3. Skin inflammation controls. For the uninfected controls, mice were infected in the shaven
338 rump above the tail with 200 µl parasite-free RPMI medium (SC). For the 'healed lesion' (HL)
339 controls, mice with *L. major* initial nodules (10 days post-inoculation, infection as described
340 above) were treated daily for 10 days with 50 mg/kg paromomycin sulphate in PBS (200 µl via
341 the intraperitoneal (IP) route). This regimen has proven efficacy in the *L. major*-BALB/c model
342 of CL (40). A size of 0 mm (complete disappearance of the skin lesion) was considered a
343 near-complete healing and a negative control for skin inflammation. For the 'pseudolesion'
344 (PL) control, mice were SC injected in the shaven rump above the tail with 25 µl 0.5 % λ-
345 carrageenan in PBS. After 24 hours, when a measurable lesion-like but parasite-free swelling

346 of skin had occurred, the pseudolesion was considered a positive control for skin
347 inflammation. These specific concentration and time points were chosen based on similarity
348 to CL-lesions and experimental requirements. The resulting diameter of the skin swelling
349 (“lesion size”) was between 2-8 mm (the size of our CL lesions). Moreover, the local
350 inflammation remained for at least 48 hours (24 hours to reach maximal swelling and another
351 24 hours for PK experiment). This novel carrageenan-induced model of local rump skin
352 inflammation in mice was based on the well-established model of rat paw inflammation (38,
353 39) and preparatory studies are shown in Supplement 1.

354 **Procedures per experimental group.** Ten mice per group (*L. major* papule, *L. major* initial nodule
355 and *L. major* established nodule; *L. mexicana* papule, *L. mexicana* initial nodule and *L. mexicana*
356 established nodule; uninfected, pseudolesion and healed lesion) were divided in a pharmacokinetic
357 (n=5) and skin pathophysiology arm (n=5). This allowed simultaneous studying of drug accumulation
358 24 hours after LAmB administration (this time point results in maximal AmB accumulation in skin(21))
359 and pathophysiology factors affecting pharmacokinetics at the time of drug administration (30 minutes
360 after administration of Evans Blue, standard time for preferential distribution of the dye to inflamed
361 compared to healthy peripheral tissue sites (35-37)). An overview of the procedures performed per
362 group is shown in figure 1.

- 363 • **Pharmacokinetic arm.** Each animal in this arm (n=5) received an IV bolus (200 µl) of LAmB
364 at a dose level of 25 mg/kg. Twenty-four hours later, animals were sacrificed and skin
365 samples (from lesion and healthy control site) were collected. The skin samples were
366 homogenised and AmB levels in tissues measured as previously described (21, 33). Briefly,
367 skin tissues were ground mechanically with zirconium oxide beads in 1 ml of PBS. The drug
368 (AmB) was then extracted from tissue homogenates with 84:16 methanol:DMSO, followed by
369 LC-MS/MS quantification. When the expression ‘AmB levels’ or ‘AmB concentrations’ is used
370 in this work without further clarification, it refers to total (liposomal + protein-bound + ‘free’)
371 amount of AmB per gram of tissue. Pharmidex Pharmaceutical Services Ltd. performed LC-
372 MS/MS analysis of the samples. The lower limit of quantification was 1 ng/ml.
- 373 • **Skin pathophysiology arm.** Each animal in this arm (n=5) received an intravenous bolus
374 (200 µl) of 0.5 % Evans Blue (Sigma, UK). Lesion size (average of width and length, mm) was
375 measured with digital callipers. Thirty minutes later, animals were sacrificed and skin samples

376 (from the lesion and the healthy control site) were collected. These samples were cut into
377 three equal parts, weighed and used for the following evaluations:

- 378 1. Capillary leakiness. The first skin fragment was used to evaluate blood vessel leakiness
379 with the Evans Blue assay. Evans Blue is a blue dye, which is, under normal
380 physiological conditions, predominantly restricted to the blood stream because of high
381 plasma protein binding. However, the protein-dye complex can extravasate at sites of
382 increased vessel leakiness, as is the case in local inflammation. Hence, the amount of
383 Evans Blue per gram of tissue is a marker for local vascular permeability (35-37). To
384 extract Evans Blue from skin, tissue sections were placed in 500 μ l formamide in
385 Eppendorf tubes and incubated in a 55 °C water bath. After 24 hours, tubes were
386 centrifuged for 10 minutes at 15000 rpm at 4 °C and supernatants were collected.
387 Absorbance (maximum 620 nm, minimum 740 nm) was determined with a Spectramax
388 M3 plate reader (Molecular Devices, UK). Samples, blanks (formamide) and calibration
389 standards (1:2 serial dilution of 100 μ g/ml Evans Blue in formamide) were measured in
390 96-well plates (200 μ l volumes). After correction against the blank, the amount of Evans
391 Blue in samples was expressed per gram of skin tissue.
- 392 2. Parasite load. The second skin tissue fragment was used to evaluate *L. major* and *L.*
393 *mexicana* parasite loads with DNA-based quantitative PCR, as described previously (40).
394 In brief, skin tissue was homogenised and DNA extracted with a Qiagen DNeasy® kit for
395 blood and tissue. Two μ l DNA extract samples (1/100 diluted) were amplified in 10 μ l
396 reactions in the presence of 5 μ l SensiFAST SYBR® NO-ROX master mix, 0.25 μ M
397 probe and 0.4 μ M primers. Triplicates of standards (10^8 to 10^2) and duplicates of
398 unknown samples were included. The tubes were placed in a 72 sample rotor of the
399 RotorGene 3000, set at 40 cycles at a denaturation setting of 95 °C for 5 minutes
400 followed by a 2-step amplification cycle of 95 °C for 10 seconds and 60 °C for 30
401 seconds. The lower limit of quantification was 100 parasites per 2 μ l.
- 402 3. Skin histomorphometry. The third and final skin fragment was fixed in formalin for 24
403 hours, dehydrated in ethanol, cleared in xylene and embedded in paraffin. Skin samples
404 were stained with haematoxylin and eosin (H&E) or antibodies against the
405 macrophage/microglia-specific protein iba-1 (anti-Iba 1). All histological procedures were

406 performed at the Institute of Neurology (UCL, London, UK) and blind analysis using the
407 same analyst was conducted at LSHTM. Leica ST5020 Autostainer was used for H&E
408 stain, according to the standard NHS diagnostic protocol. Randomly selected images
409 covering skin regions were acquired with a camera (Leica DFC295) attached to a Leica
410 DM3000 LED microscope. Images were digitalized for histomorphometric analysis using
411 the Leica Application Suite V4.5 software. An index of inflammatory cells was assessed
412 by quantifying a standardized test area of 166970.7 μm^2 per image acquired, with 20x
413 objective. The number of cells/image was determined from the average of 6
414 images/animal, randomly chosen, at 200x magnification, stained with H&E. An increase in
415 the number of cells compared with uninfected controls was considered indicative of
416 inflammation. Immunohistochemistry reaction for macrophage presence was performed
417 using the Ventana Discovery XT using the Ventana DAB Map detection Kit. Tissues were
418 pre-treated for 40 minutes with EDTA buffer, incubated for 4 hours with the primary
419 antibody (anti-Iba-1, 1/250 dilution, Wako Laboratory Chemicals, Germany) and treated
420 with Swine anti Rabbit Dako E0353 for 1 hour (manufacturers protocol). The polyclonal
421 antibodies in the anti-Iba-1 stain label the calcium-binding protein iba-1, specific to
422 microglia (central nervous system) and macrophages (skin and other tissues). An index of
423 macrophage was assessed by quantifying a standardized test area of 166970.7 μm^2 per
424 image, acquired with 20 x objective. The area in brown was determined from an average
425 of 6 randomly chosen images/animal, at 200x magnification. Increased stained area
426 compared with uninfected controls was considered indicative of macrophage infiltration.

427 **Efficacy of LAmB against *L. major* and *L. mexicana*.** Uninfected or *Leishmania*-infected BALB/c
428 mice with nodular CL lesions (10 and 30 days post-inoculation for *L. major* and *L. mexicana*,
429 respectively) received five doses (200 μl , IV) of either 5% dextrose (untreated control) or LAmB at 25
430 mg/kg (treated) on alternate days (i.e. on day 0, 2, 4, 6, 8). During treatment, lesion size was
431 monitored daily. On day 10, animals were sacrificed, lesion samples were collected and parasite load
432 and AmB drug levels in these tissues quantified (see above).

433 **Statistical analysis.** For the PK and pathophysiology experiments, intralesional AmB accumulation,
434 lesion size, parasite load, capillary leakiness, cell number and macrophage abundance were
435 compared in infected and uninfected skin of the same mice using a 2-way ANOVA followed by Sidak

436 multiple comparison test. For the efficacy experiment, ANOVA (1-way for parasite load and
 437 intralésional AmB levels, 2-way repeated measures for lesion size) followed by Tukey's multiple
 438 comparison test was used. Data is presented as mean and standard error of the mean (SEM). A p-
 439 value < 0.05 was considered statistically significant. All analyses were performed with GraphPad
 440 Prism version 7.02.

441

442 TABLES

443 Table 1: Lesion-over-healthy-skin-ratios, based on the values found in lesions (rump) and healthy
 444 control skin (back) for the following of the variables: AmB accumulation, blood vessel permeability,
 445 total number of cells, and number of macrophages. Data derived from figures 2, 4 and 5.

446

	<i>L. major</i> CL			<i>L. mexicana</i> CL			Controls		
	papule	initial nodule	establishe d nodule	papule	initial nodule	establishe d nodule	Uninf	PL (+)	HL (-)
AmB accumulation	16.2	2.5	1.2	3.7	2	1.6	0.5	3.2	0.5
Blood vessel permeability	5.9	9.4	6.8	2.6	12.5	9.5	1.7	11.7	1.2
Number of cells	1.8	2.3	2.4	1.2	1.2	1.4	1	1.6	1.1
Number of macrophage s	5.4	7.2	5.1	3	4.8	4.9	0.9	1.5	4.8

447

448 FIGURES

449 **Figure 1:** Schematic overview of experimental design to study the influence of skin inflammation in
 450 CL on the PK of LAmB.

451 **Figure 2:** Skin accumulation of amphotericin B (AmB), 24 hours after a single intravenous (IV)
452 administration of 25 mg/kg AmBisome (LAmB) to CL-infected mice at different time points post-
453 infection and controls. Drug levels were determined in the lesion (●) and healthy control skin (○) site
454 for each animal. CL-infected mice with skin lesions were dosed with LAmB at the time when a papule,
455 an initial nodule or an established nodule was present on the rump (respectively: 5, 10 and 20 days
456 after *L. major* infection; 15, 30 and 45 days after *L. mexicana* infection). Controls for skin
457 inflammation: uninfected mice (uninf), pseudolesion PL (mice with carrageenan-induced inflammatory
458 skin initial nodule) and healed lesion HL (mice with paromomycin-cured *L. major* initial nodule). Data:
459 means \pm SEM (n=3-5 per group). Statistical analysis: 2-way ANOVA followed by Sidak multiple
460 comparison test. *= p<0.05, **= p <0.01, ***= p<0.001, ****= p<0.0001.

461 **Figure 3:** Lesion size (top row) and parasite load (bottom row) in to CL-infected mice at different time
462 points post-infection and controls. Lesion size (mm) and parasite load (parasites per gram skin) were
463 determined in the lesion (●) and healthy control skin (○) for each animal. CL-infected mice with skin
464 lesions were measured at the time when a papule, an initial nodule or an established nodule was
465 present on the rump (respectively: 5, 10 and 20 days after *L. major* infection; 15, 30 and 45 days after
466 *L. mexicana* infection). Controls for skin inflammation: uninfected mice (uninf), pseudolesion PL (mice
467 with carrageenan-induced inflammatory skin initial nodule) and healed lesion HL (mice with
468 paromomycin-cured *L. major* initial nodule). Data: means \pm SEM (n=3-5 per group). Statistical
469 analysis: 2-way ANOVA followed by Sidak multiple comparison test. *= p<0.05, **= p <0.01, ***=
470 p<0.001, ****= p<0.0001.

471 **Figure 4:** Leakiness of the bloods vessels in the skin of CL-infected mice at different time points post-
472 infection and controls. After administration of Evans Blue (200 μ l 0.5%, IV), the amount of the blue
473 dye per gram of tissue was determined in the lesion (●) and healthy control skin (○) for all animals.
474 CL-infected mice with skin lesions were dosed with Evans Blue at the time when a papule, an initial
475 nodule or an established nodule was present on the rump (respectively: 5, 10 and 20 days after *L.*
476 *major* infection; 15, 30 and 45 days after *L. mexicana* infection). Controls for skin inflammation:
477 uninfected mice (uninf), pseudolesion PL (mice with carrageenan-induced inflammatory skin initial
478 nodule) and healed lesion HL (mice with paromomycin-cured *L. major* initial nodule). Data: means \pm
479 SEM (n=3-5 per group). Statistical analysis: 2-way ANOVA followed by Sidak multiple comparison

480 test. *= p<0.05, **= p <0.01, ***= p<0.001, ****= p<0.0001. The picture shows *L. major*-infected mice
481 (day 10) after 30 minutes after administration of Evans Blue (IV). The arrows point at the blue
482 coloration of the CL lesions (before skin sample collection, left photo) as well as intense blue staining
483 of the underlying thoracolumbar fascia (after skin sample collection, right photo).

484 **Figure 5:** Estimation of the number of cells (top row, H&E stain) and macrophages (bottom row, anti
485 Iba-1-reaction) at the infected lesion site (rump skin, black bars) and the control site (back skin, white
486 bars) of control mice and CL-infected mice. Measurements in CL-infected mice with skin lesions were
487 performed at the time when a papule, an initial nodule or an established nodule was present on the
488 rump (respectively: 5, 10 and 20 days after *L. major* infection; 15, 30 and 45 days after *L. mexicana*
489 infection). Controls for skin inflammation: uninfected mice (uninf), pseudolesion PL (mice with
490 carrageenan-induced inflammatory skin initial nodule) and healed lesion HL (mice with paromomycin-
491 cured *L. major* initial nodule). Standard surface: picture area showing full skin tissue (epidermis,
492 dermis and hypodermis) to allow direct comparisons among groups (166970.7 μm^2). Data: means \pm
493 SEM (n=3-5 per group). Statistical analysis: 2-way ANOVA followed by Sidak multiple comparison
494 test. *= p<0.05, **= p <0.01, ***= p<0.001, ****= p<0.0001.

495 **Figure 6:** Collage panels of murine skin lesions developed during CL disease progress and controls
496 for skin inflammation. Per panel: photo of the lesion on the rump of the mice (a, white arrow points at
497 lesion), haematoxylin and eosin stain (b, purple arrow points at a cluster of inflammatory cells) and
498 macrophage marker anti-ionized calcium binding adapter molecule 1-antibody stain (c, brown arrow
499 points at a cluster of macrophages). Top row: controls for skin inflammation (uninfected, pseudolesion
500 and healed lesion). Middle row: *L. major* CL lesions (papule present 5 days post-infection, initial
501 nodule present 10 days post-infection and an established nodule present 20 days post-infection).
502 Bottom row: *L. mexicana* CL lesions (papule present 15 days post-infection, initial nodule present 30
503 days post-infection and an established nodule present 45 days post-infection). Black bar in (b) = 100
504 μm .

505 **Figure 7:** Comparison of mouse skin morphology and macrophage density in healthy, uninfected skin
506 (left), *L. major* CL lesion (20 days post-infection, middle) and *L. mexicana* CL lesion (45 days post-
507 infection, right). The central picture in each panel (H&E stain) shows the structural layers of the skin:
508 epidermis (E), dermis (D) and hypodermis (H), with the underlying muscle (M) at x 4 magnification

509 (bar = 100 μm). The inserts (1-4) highlight details of the central picture (x 80 magnification, bar =10
510 μm). ①: epidermis. ②: dermal capillaries. ③: *Leishmania* amastigotes within parasitophorous
511 vacuoles. ④: anti-iba-1 stain (macrophage marker) of tissue shown in insert ③. In both the *L. major*
512 and *L. mexicana* CL lesion, intense inflammatory foci (I) are present in the skin, causing severe
513 disruption the D and H architecture. Compared to healthy, uninfected skin, CL lesions also showed (i)
514 epidermal hyperplasia and acanthosis for *L. mexicana* but not for *L. major* (①), (ii) dilated blood
515 vessels, a factor contributing to capillary leakiness (②) and (iii) a large amount of inflammatory cells
516 (③), many of which are macrophages (④).

517 **Figure 8:** Efficacy and biodistribution of liposomal amphotericin B LAmB) in murine models *L. major*
518 and *L. mexicana* CL. Mice were injected (SC) with parasite-free medium (uninfected) or infected with
519 *L. major* or *L. mexicana* promastigotes in the rump skin. When a nodular lesion had formed at the
520 inoculation site of CL-infected animals (10 and 30 days post-inoculation for *L. major* and *L. mexicana*,
521 respectively), animals received either 5% dextrose (untreated) or 25 mg/kg LAmB (IV) on days 0, 2, 4,
522 6 and 8. During treatment, lesion size (a) was measured daily. On day 10, lesion skin tissues were
523 collected and parasite load (b) and AmB levels (c) determined. Each point represents mean \pm SEM
524 (n=3-5 per group). ANOVA (1-way for parasite load and intralésional AmB levels, repeated measures
525 for lesion size), followed by Tukey's multiple comparison test (* = $p < 0.05$, **** = $p < 0.0001$, ns = not
526 significant). N/A: not applicable.

527

528 ACKNOWLEDGEMENTS

529 Gert-Jan Wijnant's doctoral project is part of the EuroLeish.Net Training Network (www.euroleish.net).
530 This work was supported by the European Horizon's 2020 Research and Innovation Programme
531 under the Marie Skłodowska-Curie grant agreement number 642609.

532

533 REFERENCES

- 534 1. Okwor I, Uzonna J. 2016. Social and Economic Burden of Human Leishmaniasis. Am J Trop
535 Med Hyg 94:489–493.

- 536 2. Alvar J, Vélez ID, Bern C, Herrero M, Desjeux P, Cano J, Jannin J, den Boer M. 2012.
537 Leishmaniasis Worldwide and Global Estimates of Its Incidence. *PLoS One* 7.
- 538 3. Scorza BM, Carvalho EM, Wilson ME. 2017. Cutaneous Manifestations of Human and Murine
539 Leishmaniasis. *Int J Mol Sci* 18.
- 540 4. Scott P, Novais FO. 2016. Cutaneous leishmaniasis: immune responses in protection and
541 pathogenesis. *Nat Rev Immunol* 16:581–592.
- 542 5. Cangussú SD, Souza CC de, Campos CF, Vieira LQ, Afonso LCC, Arantes RME. 2009.
543 Histopathology of *Leishmania major* infection: revisiting *L. major* histopathology in the ear
544 dermis infection model. *Mem Inst Oswaldo Cruz* 104:918–922.
- 545 6. Corware K, Harris D, Teo I, Rogers M, Naresh K, Müller I, Shaunak S. 2011. Accelerated
546 healing of cutaneous leishmaniasis in non-healing BALB/c mice using water soluble
547 amphotericin B-polymethacrylic acid. *Biomaterials* 32:8029–8039.
- 548 7. Gaafar A, el Kadar AY, Theander TG, Permin H, Ismail A, Kharazmi A, el Hassan AM. 1995.
549 The pathology of cutaneous leishmaniasis due to *Leishmania major* in Sudan. *Am J Trop Med*
550 *Hyg* 52:438–442.
- 551 8. Andrade ZA, Reed SG, Roters SB, Sadigursky M. 1984. Immunopathology of experimental
552 cutaneous leishmaniasis. *Am J Pathol* 114:137–148.
- 553 9. Kaye PM, Beattie L. 2016. Lessons from other diseases: granulomatous inflammation in
554 leishmaniasis. *Semin Immunopathol* 38:249–260.
- 555 10. Nylén S, Eidsmo L. 2012. Tissue damage and immunity in cutaneous leishmaniasis. *Parasite*
556 *Immunol* 34:551–561.
- 557 11. Mehregan DR, Mehregan AH, Mehregan DA. 1999. Histologic diagnosis of cutaneous
558 leishmaniasis. *Clin Dermatol* 17:297–304.
- 559 12. Bari AU. 2012. Clinical spectrum of cutaneous leishmaniasis: an overview from Pakistan.
560 *Dermatol Online J* 18:4.
- 561 13. Abuzaid AA, Abdoon AM, Aldahan MA, Alzahrani AG, Alhakeem RF, Asiri AM, Alzahrani MH,
562 Memish ZA. 2017. Cutaneous Leishmaniasis in Saudi Arabia: A Comprehensive Overview.
563 *Vector Borne Zoonotic Dis* 17:673–684.
- 564 14. Blaylock JM, Wortmann GW. 2012. A case report and literature review of “Chiclero’s Ulcer”.
565 *Travel Med Infect Dis* 10:275–278.

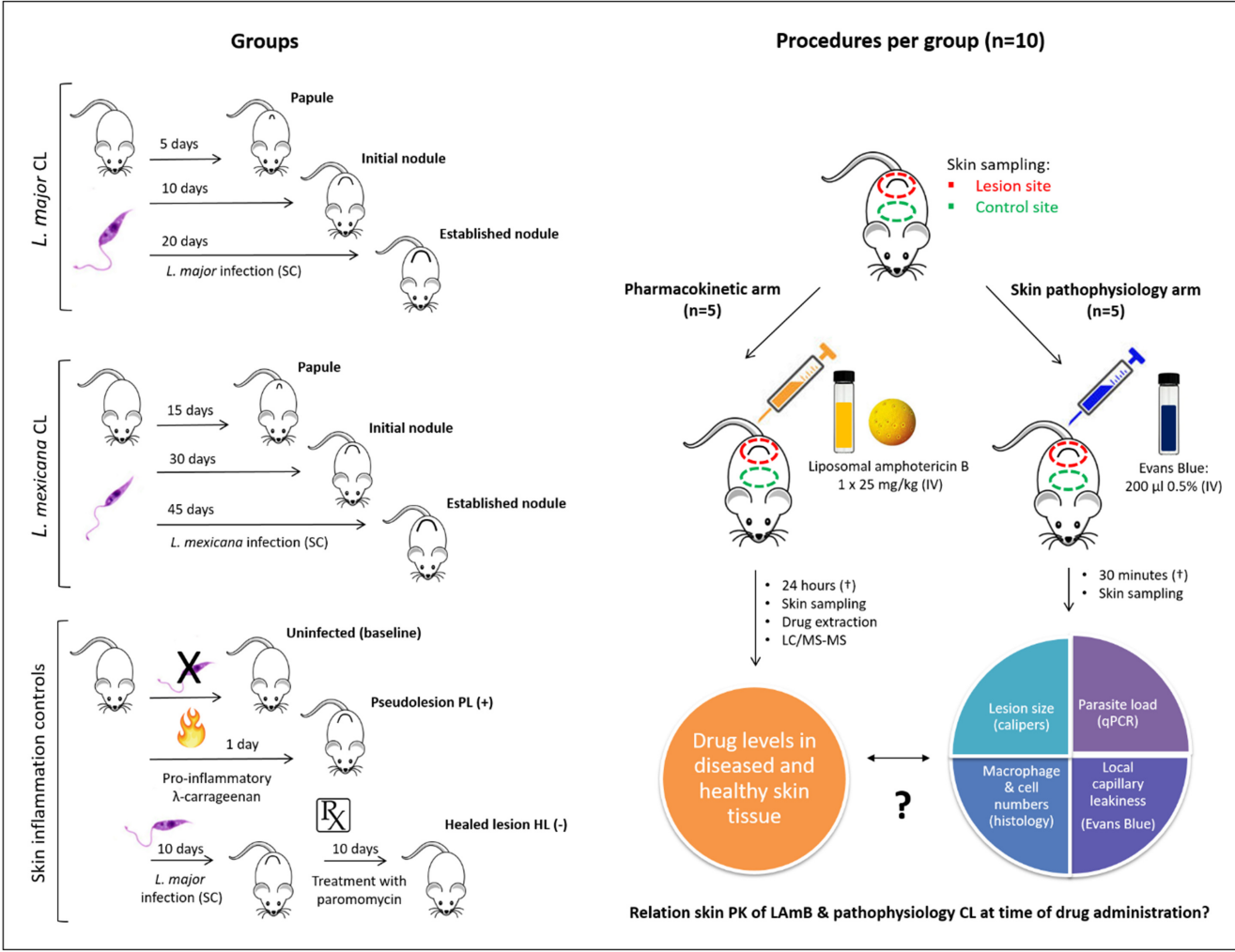
- 566 15. Calvopiña M, Martínez L, Hashiguchi Y. 2013. Cutaneous leishmaniasis “chiclero’s ulcer” in
567 subtropical Ecuador. *Am J Trop Med Hyg* 89:195–196.
- 568 16. Hodiamont CJ, Kager PA, Bart A, de Vries HJC, van Thiel PPAM, Leenstra T, de Vries PJ,
569 van Vugt M, Grobusch MP, van Gool T. 2014. Species-Directed Therapy for Leishmaniasis in
570 Returning Travellers: A Comprehensive Guide. *PLoS Negl Trop Dis* 8.
- 571 17. Balasegaram M, Ritmeijer K, Lima MA, Burza S, Ortiz Genovese G, Milani B, Gaspani S,
572 Potet J, Chappuis F. 2012. Liposomal amphotericin B as a treatment for human
573 leishmaniasis. *Expert Opin Emerg Drugs* 17:493–510.
- 574 18. Wortmann G, Zapor M, Ressler R, Fraser S, Hartzell J, Pierson J, Weintrob A, Magill A.
575 2010. Liposomal Amphotericin B for Treatment of Cutaneous Leishmaniasis. *Am J Trop Med*
576 *Hyg* 83:1028–1033.
- 577 19. Aronson N, Herwaldt BL, Libman M, Pearson R, Lopez-Velez R, Weina P, Carvalho E,
578 Ephros M, Jeronimo S, Magill A. 2017. Diagnosis and Treatment of Leishmaniasis: Clinical
579 Practice Guidelines by the Infectious Diseases Society of America (IDSA) and the American
580 Society of Tropical Medicine and Hygiene (ASTMH). *Am J Trop Med Hyg* 96:24–45.
- 581 20. Guery R, Henry B, Martin-Blondel G, Rouzaud C, Cordoliani F, Harms G, Gangneux J-P,
582 Foulet F, Bourrat E, Baccard M, Morizot G, Consigny P-H, Berry A, Blum J, Lortholary O,
583 Buffet P. 2017. Liposomal amphotericin B in travelers with cutaneous and muco-cutaneous
584 leishmaniasis: Not a panacea. *PLoS Negl Trop Dis* 11.
- 585 21. Wijnant G-J, Van Bocxlaer K, Yardley V, Harris A, Murdan S, Croft SL. 2018. Relation
586 between Skin Pharmacokinetics and Efficacy in AmBisome Treatment of Murine Cutaneous
587 Leishmaniasis. *Antimicrob Agents Chemother* 62.
- 588 22. Felton T, Troke PF, Hope WW. 2014. Tissue Penetration of Antifungal Agents. *Clin Microbiol*
589 *Rev* 27:68–88.
- 590 23. Ternant D, Ducourau E, Perdriger A, Corondan A, Le Goff B, Devauchelle-Pensec V, Solau-
591 Gervais E, Watier H, Goupille P, Paintaud G, Mulleman D. 2014. Relationship between
592 inflammation and infliximab pharmacokinetics in rheumatoid arthritis. *Br J Clin Pharmacol*
593 78:118–128.

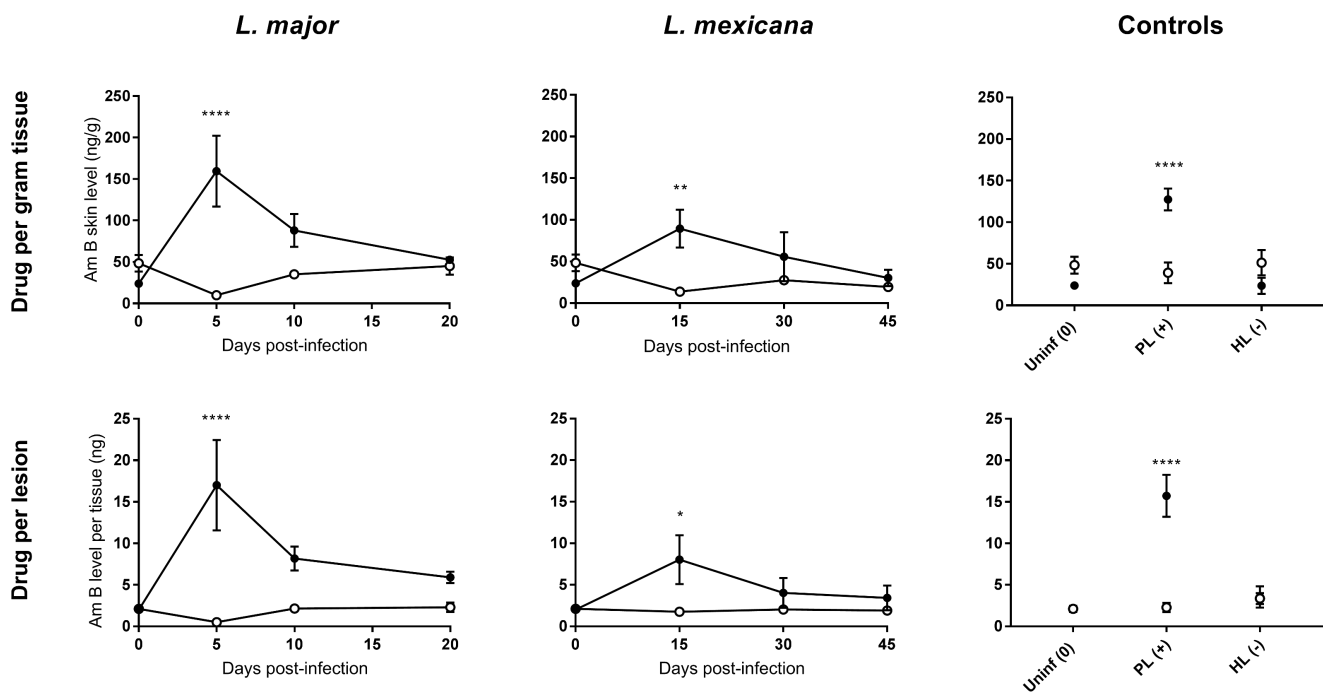
- 594 24. Slaviero KA, Clarke SJ, Rivory LP. 2003. Inflammatory response: an unrecognised source of
595 variability in the pharmacokinetics and pharmacodynamics of cancer chemotherapy. *Lancet*
596 *Oncol* 4:224–232.
- 597 25. Wu NZ, Da D, Rudoll TL, Needham D, Whorton AR, Dewhirst MW. 1993. Increased
598 microvascular permeability contributes to preferential accumulation of Stealth liposomes in
599 tumor tissue. *Cancer Res* 53:3765–3770.
- 600 26. Poh S, Chelvam V, Low PS. 2015. Comparison of nanoparticle penetration into solid tumors
601 and sites of inflammation: studies using targeted and nontargeted liposomes. *Nanomedicine*
602 (Lond) 10:1439–1449.
- 603 27. Blot SI, Pea F, Lipman J. 2014. The effect of pathophysiology on pharmacokinetics in the
604 critically ill patient--concepts appraised by the example of antimicrobial agents. *Adv Drug*
605 *Deliv Rev* 77:3–11.
- 606 28. Sykes EA, Dai Q, Tsoi KM, Hwang DM, Chan WCW. 2014. Nanoparticle exposure in animals
607 can be visualized in the skin and analyzed via skin biopsy. *Nat Commun* 5:3796.
- 608 29. Mehta RT, McQueen TJ, Keyhani A, López-Berestein G. 1994. Phagocyte Transport as
609 Mechanism for Enhanced Therapeutic Activity of Liposomal Amphotericin B. *CHE* 40:256–
610 264.
- 611 30. Girard AE, Cimochoowski CR, Faiella JA. 1996. Correlation of increased azithromycin
612 concentrations with phagocyte infiltration into sites of localized infection. *J Antimicrob*
613 *Chemother* 37 Suppl C:9–19.
- 614 31. Drusano GL. 2005. Infection site concentrations: their therapeutic importance and the
615 macrolide and macrolide-like class of antibiotics. *Pharmacotherapy* 25:150S-158S.
- 616 32. Kelly C, Jefferies C, Cryan S-A. 2011. Targeted Liposomal Drug Delivery to Monocytes and
617 Macrophages. *J Drug Deliv* 2011.
- 618 33. Voak AA, Harris A, Qaiser Z, Croft SL, Seifert K. 2017. Pharmacodynamics and
619 Biodistribution of Single-Dose Liposomal Amphotericin B at Different Stages of Experimental
620 Visceral Leishmaniasis. *Antimicrob Agents Chemother* 61.
- 621 34. Lasic DD, Papahadjopoulos D. 1995. Liposomes revisited. *Science* 267:1275–1276.
- 622 35. Radu M, Chernoff J. 2013. An in vivo assay to test blood vessel permeability. *J Vis Exp*
623 e50062.

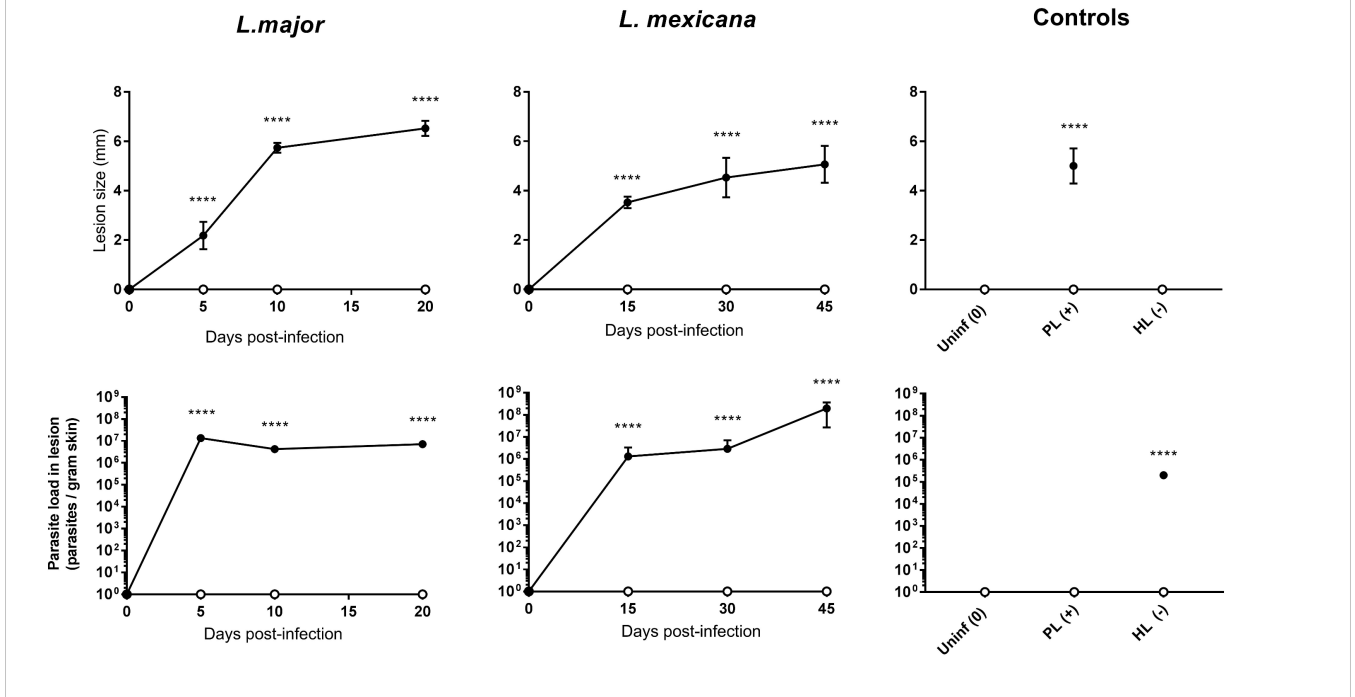
- 624 36. Nidavani RB, Am M, Shalawadi M. 2014. Vascular permeability and Evans blue dye: a
625 physiological and pharmacological approach -. *Journal of Applied Pharmaceutical Science*
626 4:106–113.
- 627 37. krzyzanowska agi, Martin Y, Avendaño C, Piedras MJ, Krzyzanowska A. 2010. Evaluation of
628 Evans Blue extravasation as a measure of peripheral inflammation. *Protocol Exchange*.
- 629 38. Fehrenbacher JC, Vasko MR, Duarte DB. 2012. Models of Inflammation: Carrageenan- or
630 Complete Freund's Adjuvant-Induced Edema and Hypersensitivity in the Rat. *Curr Protoc*
631 *Pharmacol 0 5:Unit5.4*.
- 632 39. Morris CJ. 2003. Carrageenan-induced paw edema in the rat and mouse. *Methods Mol Biol*
633 225:115–121.
- 634 40. Wijnant G-J, Van Bocxlaer K, Yardley V, Murdan S, Croft SL. 2017. Efficacy of Paromomycin-
635 Chloroquine Combination Therapy in Experimental Cutaneous Leishmaniasis. *Antimicrob*
636 *Agents Chemother* 61.
- 637 41. Brajtburg J, Bolard J. 1996. Carrier effects on biological activity of amphotericin B. *Clin*
638 *Microbiol Rev* 9:512–531.
- 639 42. Lestner JM, Howard SJ, Goodwin J, Gregson L, Majithiya J, Walsh TJ, Jensen GM, Hope
640 WW. 2010. Pharmacokinetics and Pharmacodynamics of Amphotericin B Deoxycholate,
641 Liposomal Amphotericin B, and Amphotericin B Lipid Complex in an In Vitro Model of Invasive
642 Pulmonary Aspergillosis. *Antimicrob Agents Chemother* 54:3432–3441.
- 643 43. Lopez-Berestein G, Rosenblum MG, Mehta R. 1984. Altered tissue distribution of
644 amphotericin B by liposomal encapsulation: comparison of normal mice to mice infected with
645 *Candida albicans*. *Cancer Drug Deliv* 1:199–205.
- 646 44. Alexander J, Kaye PM. 1985. Immunoregulatory pathways in murine leishmaniasis: different
647 regulatory control during *Leishmania mexicana mexicana* and *Leishmania major* infections.
648 *Clin Exp Immunol* 61:674–682.
- 649 45. El-On J, Lang E, Kuperman O, Avinoach I. 1989. *Leishmania major*: histopathological
650 responses before and after topical treatment in experimental animals. *Exp Parasitol* 68:144–
651 154.

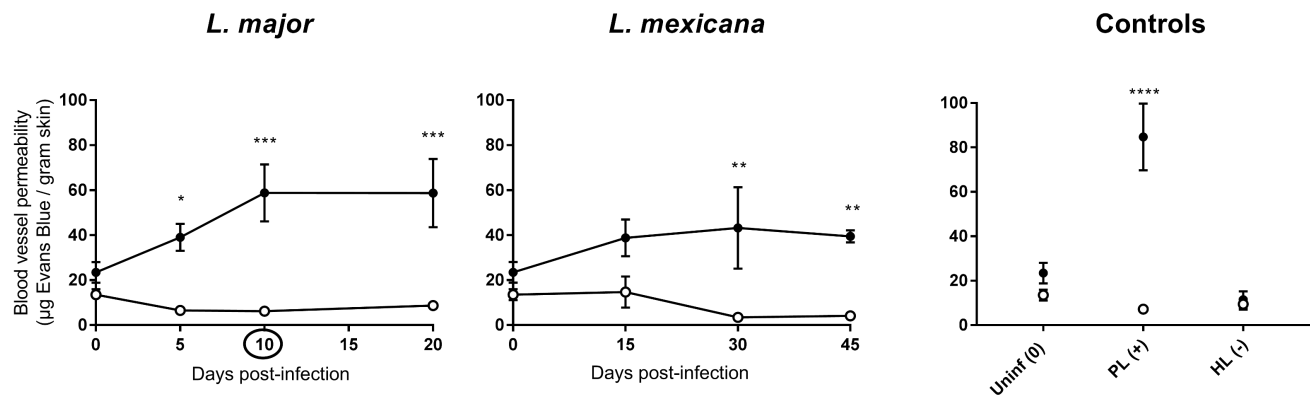
- 652 46. Clay GM, Valadares DG, Graff JW, Ulland TK, Davis RE, Scorza BM, Zhanbolat BS, Chen
653 Y, Sutterwala FS, Wilson ME. 2017. An Anti-Inflammatory Role for NLRP10 in Murine
654 Cutaneous Leishmaniasis. *J Immunol* 199:2823–2833.
- 655 47. Andrade-Narvaez FJ, Medina-Peralta S, Vargas-Gonzalez A, Canto-Lara SB, Estrada-Parra
656 S. 2005. The histopathology of cutaneous leishmaniasis due to *Leishmania* (*Leishmania*)
657 mexicana in the Yucatan peninsula, Mexico. *Rev Inst Med Trop Sao Paulo* 47:191–194.
- 658 48. Dainichi T, Hanakawa S, Kabashima K. 2014. Classification of inflammatory skin diseases: A
659 proposal based on the disorders of the three-layered defense systems, barrier, innate
660 immunity and acquired immunity. *Journal of Dermatological Science* 76:81–89.
- 661 49. Oja CD, Semple SC, Chonn A, Cullis PR. 1996. Influence of dose on liposome clearance:
662 critical role of blood proteins. *Biochimica et Biophysica Acta (BBA) - Biomembranes* 1281:31–
663 37.
- 664 50. Varricchi G, Granata F, Loffredo S, Genovese A, Marone G. 2015. Angiogenesis and
665 lymphangiogenesis in inflammatory skin disorders. *J Am Acad Dermatol* 73:144–153.
- 666 51. Bekersky I, Fielding RM, Dressler DE, Lee JW, Buell DN, Walsh TJ. 2002. Pharmacokinetics,
667 Excretion, and Mass Balance of Liposomal Amphotericin B (AmBisome) and Amphotericin B
668 Deoxycholate in Humans. *Antimicrob Agents Chemother* 46:828–833.
- 669 52. Wijnant GJ, Van Bocxlaer K, Yardley V, Harris A, Alavijeh M, Silva-Pedrosa R, Antunes S,
670 Mauricio I, Murdan S, Croft SL. 2018. Comparative efficacy, toxicity and biodistribution of the
671 liposomal amphotericin B formulations Fungisome and AmBisome in murine cutaneous
672 leishmaniasis. Submitted to *International Journal of Parasitology*, under review.
- 673 53. Kloehn J, Saunders EC, O'Callaghan S, Dagley MJ, McConville MJ. 2015. Characterization of
674 Metabolically Quiescent *Leishmania* Parasites in Murine Lesions Using Heavy Water
675 Labeling. *PLOS Pathogens* 11:e1004683.
- 676 54. Mandell MA, Beverley SM. 2017. Continual renewal and replication of persistent *Leishmania*
677 major parasites in concomitantly immune hosts. *PNAS* 114:E801–E810.
- 678 55. Jara M, Berg M, Caljon G, de Muylder G, Cuypers B, Castillo D, Maes I, Orozco M del C,
679 Vanaerschot M, Dujardin J-C, Arevalo J. 2017. Macromolecular biosynthetic parameters and
680 metabolic profile in different life stages of *Leishmania braziliensis*: Amastigotes as a
681 functionally less active stage. *PLoS One* 12.

- 682 56. Zhao M, Lepak AJ, Andes DR. 2016. Animal models in the
683 pharmacokinetic/pharmacodynamic evaluation of antimicrobial agents. *Bioorg Med Chem*
684 24:6390–6400.
- 685 57. von Stebut E. 2007. Cutaneous Leishmania infection: progress in pathogenesis research and
686 experimental therapy. *Exp Dermatol* 16:340–346.
- 687 58. Mears ER, Modabber F, Don R, Johnson GE. 2015. A Review: The Current In Vivo Models
688 for the Discovery and Utility of New Anti-leishmanial Drugs Targeting Cutaneous
689 Leishmaniasis. *PLoS Negl Trop Dis* 9:e0003889.
- 690 59. McCormick TS, Stevens SR, Kang K. 2000. Macrophages and cutaneous inflammation.
691 *Nature Biotechnology* 18:25.
- 692 60. Pasparakis M, Haase I, Nestle FO. 2014. Mechanisms regulating skin immunity and
693 inflammation. *Nat Rev Immunol* 14:289–301.
- 694 61. Gutiérrez V, Seabra AB, Reguera RM, Khandare J, Calderón M. 2016. New approaches from
695 nanomedicine for treating leishmaniasis. *Chem Soc Rev* 45:152–168.
- 696 62. Antonio L de F, Fagundes A, Oliveira RVC, Pinto PG, Bedoya-Pacheco SJ, Vasconcellos E
697 de CF e, Valete-Rosalino MC, Lyra MR, Passos SRL, Pimentel MIF, Schubach A de O. 2014.
698 Montenegro skin test and age of skin lesion as predictors of treatment failure in cutaneous
699 leishmaniasis. *Rev Inst Med Trop Sao Paulo* 56:375–380.
- 700 63. Machado P, Araújo C, Silva D, T A, Almeida RP, D'Oliveira A, Bittencourt A, Carvalho EM.
701 2002. Failure of Early Treatment of Cutaneous Leishmaniasis in Preventing the Development
702 of an Ulcer. *Clin Infect Dis* 34:e69–e73.
- 703 64. Van Bocxlaer K, Yardley V, Murdan S, Croft SL. 2016. Drug permeation and barrier damage
704 in Leishmania-infected mouse skin. *J Antimicrob Chemother* 71:1578–1585.
- 705 65. Van Bocxlaer K, Gaukel E, Hauser D, Park SH, Schock S, Yardley V, Randolph R, Plattner
706 JJ, Merchant T, Croft SL, Jacobs RT, Wring SA. 2018. Topical Treatment for Cutaneous
707 Leishmaniasis: Dermato-Pharmacokinetic Lead Optimization of Benzoxaboroles. *Antimicrob*
708 *Agents Chemother* 62.
- 709

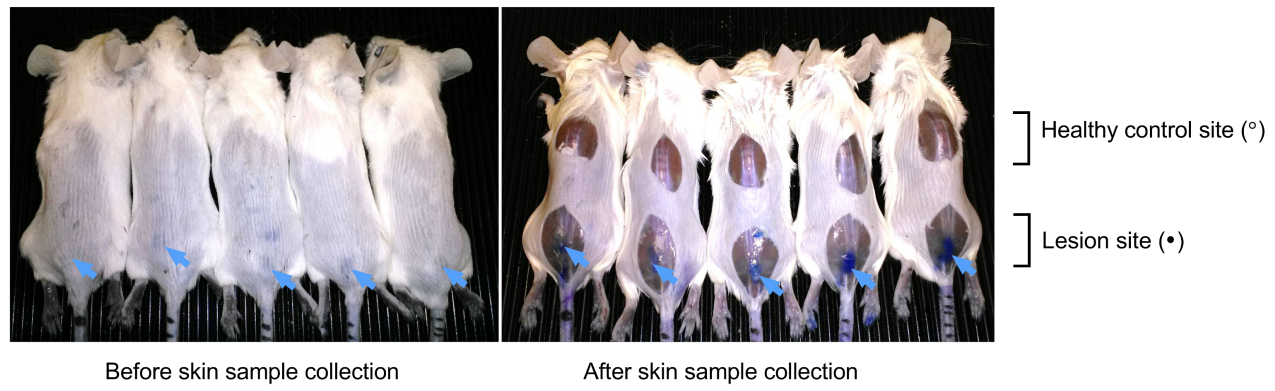


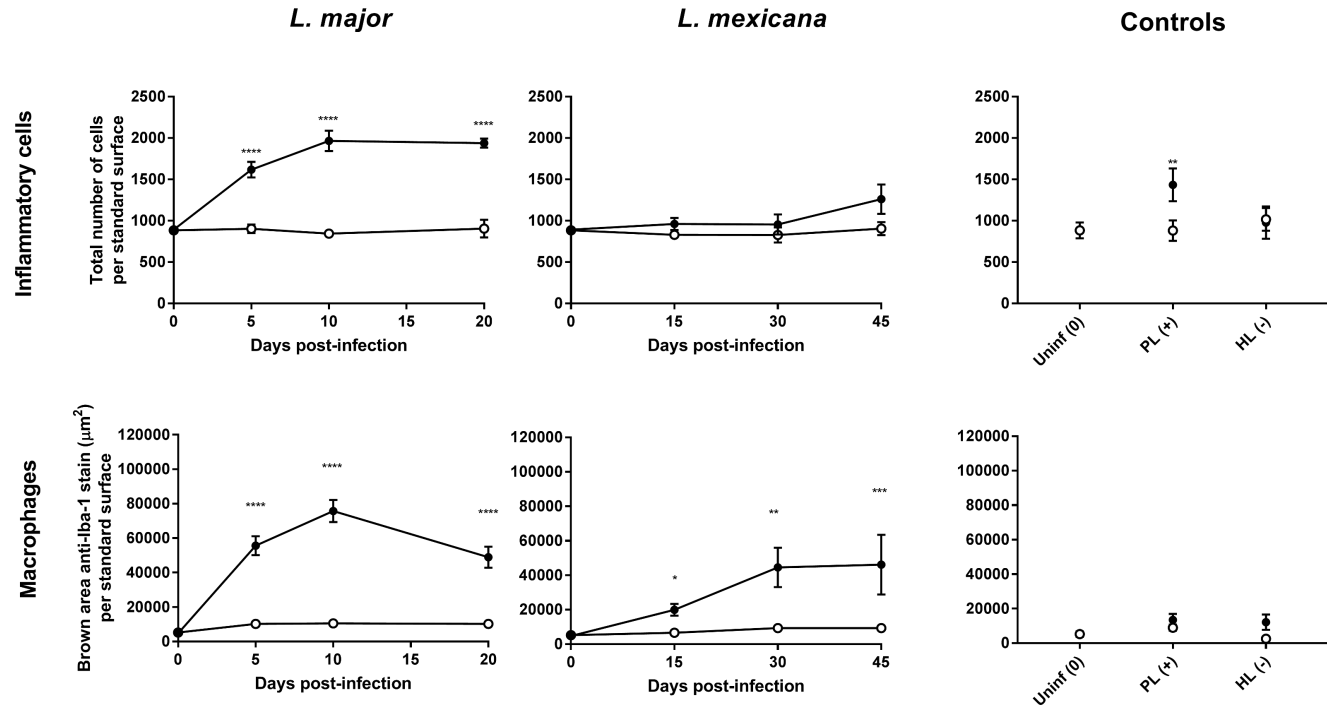


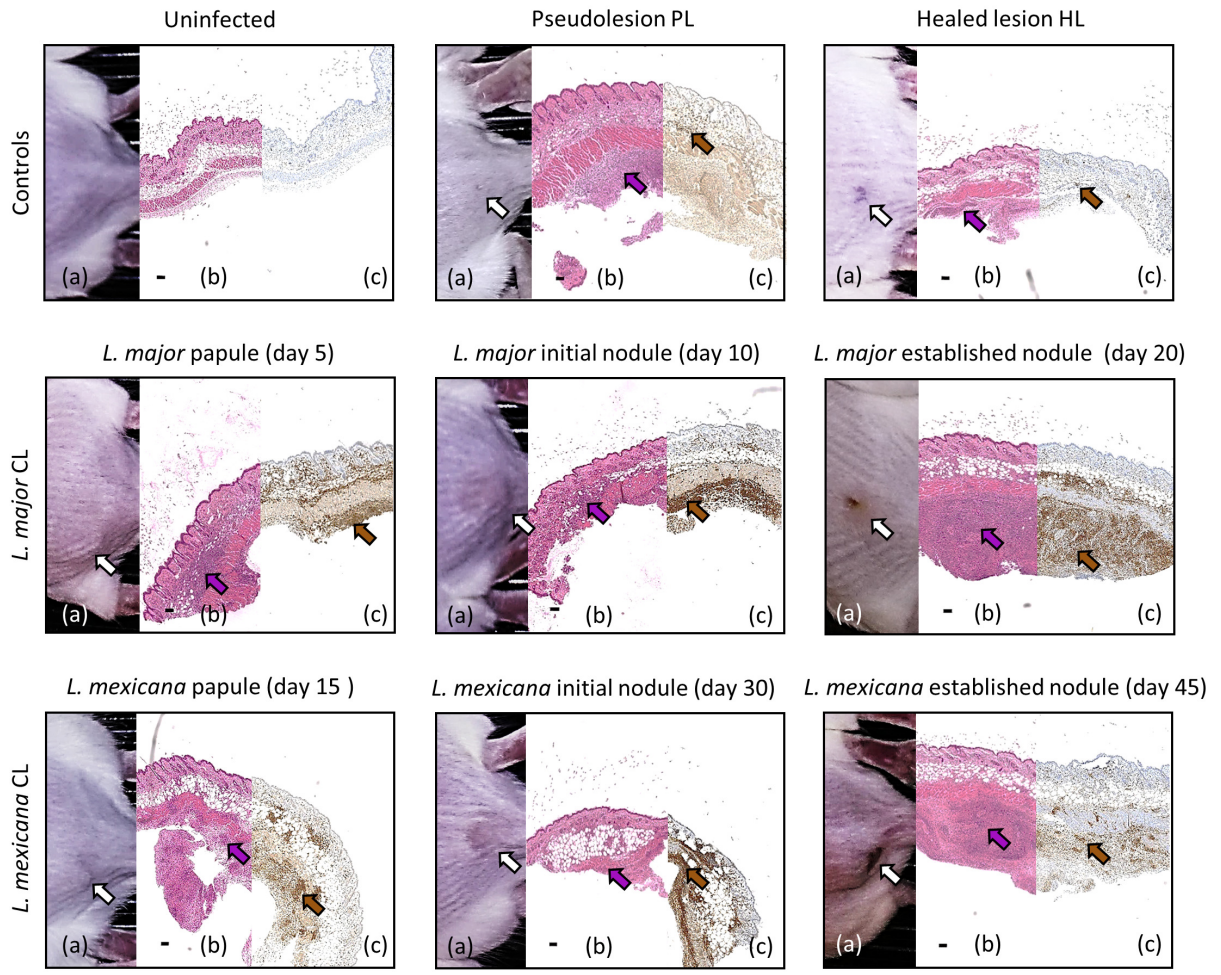




Evans Blue treated *L. major*-infected mice (day 10 post-infection):

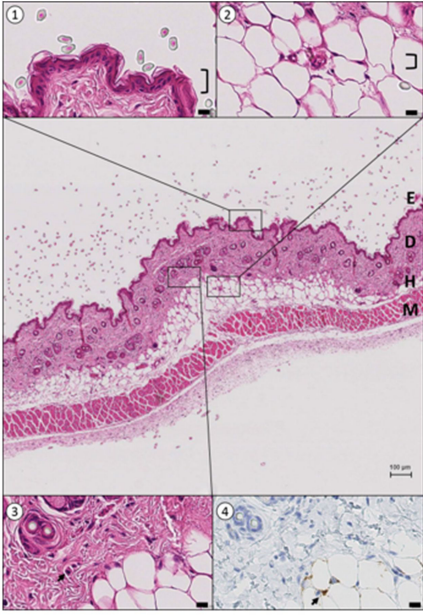




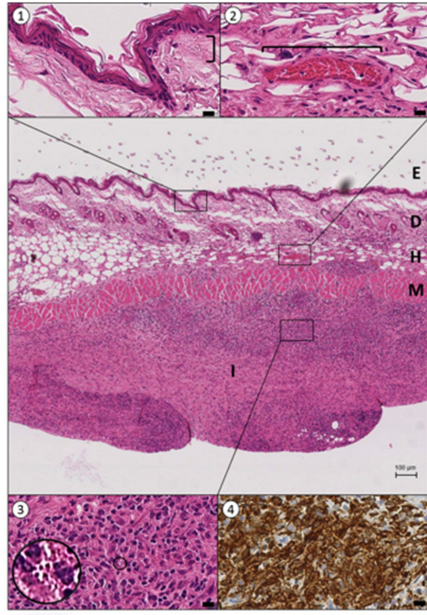


Layout per panel:

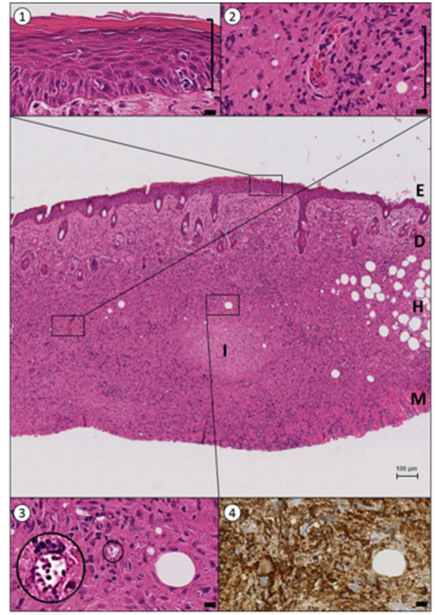
Photo lesion on mouse rump (a) = skin lesion	H&E stain lesion (b) = inflammatory infiltrate	Anti-Iba-1 stain lesion (c) = macrophage cluster
---	---	---



Healthy, uninfected skin



L. major lesion



L. mexicana lesion

